Journal of Physiology (1990), **423**, *pp.* 593–614
With 9 figures
Printed in Great Britain

A VOLTAGE-CLAMP STUDY OF THE ELECTROPHYSIOLOGICAL CHARACTERISTICS OF THE INTRAMURAL NEURONES OF THE RAT TRACHEA

BY T. G. J. ALLEN*† AND G. BURNSTOCK

From the Department of Anatomy and Developmental Biology and Centre for Neuroscience, University College London, Gower Street, London WC1E 6BT

(*Received 11 September 1989*)

SUMMARY

1. The electrophysiological characteristics of intramural neurones from the paratracheal ganglia of 14- to 18-day-old rats were studied *in vitro* using intracellular, single-electrode current- and voltage-clamp techniques.

2. Resting membrane potentials ranged between −50 and −73 mV. In 50–60% of all neurones, random and occasionally patterned bursts of spontaneous, fast synaptic potentials were observed. In all cases, superfusion with either hexamethonium (100 μM), or Ca^{2+}-free, high-magnesium-containing solutions abolished all synaptic activity.

3. Two distinct patterns of spike discharge were observed in response to prolonged intrasomal current injection. Most cells (65–75%) fired rhythmic, high-frequency (50–90 Hz) bursts of action potentials, with interburst intervals of between 300 and 500 ms, throughout the period of current stimulation. A further 10–15% of cells fired tonically at low frequencies (10–15 Hz) for the duration of the applied stimulus. In both cell types, trains of action potentials were followed by a pronounced calcium-dependent after-hyperpolarization which persisted for up to 3 s. The magnitude of the after-hyperpolarization following a single spike in tonic-firing cells was considerably larger than in burst-firing cells. Both the action potential and the after-hyperpolarization in all cells displayed a calcium-dependent, tetrodotoxin-resistant component which was abolished by the removal of extracellular calcium.

4. The spike after-hyperpolarization resulted from activation of an outward calcium-dependent potassium current which reversed at −86·5 mV. This value was shifted by 63·6 mV for a 10-fold increase in extracellular potassium concentration.

5. All of the cells studied exhibited marked outward rectification when depolarized. This resulted from activation of a time- and voltage-dependent M-current. The slow inward current relaxations associated with the M-current became faster at more negative potentials and reversed around −85 mV. Raising the extracellular potassium concentration shifted the reversal potential for the current relaxations to more depolarized potentials in a manner predicted by the Nernst equation for a current carried by potassium ions. Both the outward current at

* Present address: Department of Pharmacology, University College London, Gower Street, London WC1E 6BT.

† To whom all correspondence should be addressed.

MS 7932

depolarized potentials and the slow current relaxations were potently inhibited by extracellular $BaCl_2$ (1 mM) but were unaffected by CsCl (1–3 mM).

6. Inward rectification at hyperpolarized potentials was a characteristic of all cells. Membrane hyperpolarization revealed inward rectification in the 'instantaneous' current–voltage relationship at membrane potentials greater than −80 mV. In addition, cells also exhibited slow inward current relaxations (which did not show reversal at −85 mV) that became faster at hyperpolarized potentials, and resulted in inward rectification in the steady-state current–voltage relationship between −60 and −120 mV. The current underlying the observed relaxations showed voltage-dependent activation which became maximal at around −100 mV. The fast 'instantaneously' rectifying current was potently inhibited by extracellular CsCl (1 mM) and $BaCl_2$ (1 mM). In contrast, the slowly developing inwardly relaxing current was potently inhibited by CsCl (1 mM), but was largely resistant to $BaCl_2$ (1 mM). In the presence of CsCl (1 mM) and $BaCl_2$ (1 mM), the input resistance of paratracheal neurones was greatly increased and the current–voltage relationship became almost linear between −45 and −120 mV.

7. The roles played by the different membrane currents in the control of excitability of paratracheal neurones and the possible role of intrinsic synapses between ganglion cells are discussed.

INTRODUCTION

The existence of an extensive network of nerve fibres and large numbers of small ganglia in the walls of the trachea was first described by Landois (1885). Although there have subsequently been many studies of the extrinsic innervation of the trachea (e.g. Elfman, 1943; Honjin, 1954, 1956; Fisher, 1964; Pack, Al-Ugaily & Widdicombe, 1984), little direct evidence has been gathered to determine the role played by the intramural tracheal ganglia. The ganglia are concentrated along the posterior wall of the trachea, opposite the intervals between the cartilage rings, and make up part of an extensive plexus of nerve fibres. Branches from this network send fibres to the tracheal mucous glands, into the trachealis muscle, and also contribute to the fine plexuses accompanying the tracheal vessels (Larsell, 1922; Smith & Taylor, 1971).

Ultrastructural studies of ganglia from both the mouse and guinea-pig trachea have revealed that there are large differences in the sizes of tracheal neurones from the same animal, and it has been suggested that this may indicate the presence of more than one neuronal population (Baluk, Fujiwara & Matsuda, 1985; Chiang & Gabella, 1986). In addition, direct visualization of ferret and rat paratracheal ganglia, using acetylcholinesterase histochemistry, has revealed that there are also regional variations in the numbers and size of neurones making up these ganglia (Baker, McDonald, Basbaum & Mitchell, 1986; Baluk & Gabella, 1989).

Neural control of tracheobronchial function involves not only the classical cholinergic and adrenergic systems, but it also incorporates pathways which are neither adrenergic nor cholinergic (NANC) (Coburn & Tomita, 1973; Coleman & Levy, 1974; Richardson & Bouchard, 1975; Richardson & Beland, 1976; Diamond & O'Donnell, 1980). Evidence for the involvement of intramural neurones in NANC innervation has come from studies of the cat and guinea-pig trachea, where the

NANC component of bronchodilatation evoked by stimulation of the preganglionic vagal nerves is blocked by hexamethonium, but is unaffected by either adrenergic or muscarinic receptor blockade (Diamond & O'Donnell, 1980; Yip, Palombini & Coburn, 1981). A prime candidate for the mediation of part, if not all, of the NANC response is vasoactive intestinal polypeptide, which has been localized in intrinsic tracheal ganglion cells (Uddman, Alumets, Densert, Håkanson & Sundler, 1978; Dey, Shannon & Said, 1981). Other peptides present within and around intrinsic ganglia have also been shown to alter a number of aspects of tracheal function (for review see Lundberg & Saria, 1987). In general, however, the mechanisms by which these actions are mediated remain largely unknown.

To date, there have been relatively few direct electrophysiological studies of the neurones from the intrinsic paratracheal ganglia. The majority of these have been carried out on ferret ganglia, where 30–40% of the neurones reside within two superficial ganglionated chains, which run along the posterior wall of the trachealis muscle. In the first intracellular studies of these neurones, two cell types were reported. One type, termed AH cells, displayed pronounced spike after-hyperpolarizations, whereas a second cell type, B cells, exhibited no somal spikes, but displayed slow inhibitory and excitatory postsynaptic potentials (EPSPs) in response to preganglionic stimulation (Cameron & Coburn, 1984). Subsequent studies of ferret ganglia in general concur with these early findings (Baker, 1986; Baker *et al.* 1986; Coburn & Kalia, 1986). However, Baker and his colleagues have reported an additional type of cell capable of firing damped trains of action potentials in response to prolonged intrasomal current injection (Baker *et al.* 1986). In an *in vivo* study of the cat, spike discharge in paratracheal neurones has been shown to parallel activity in the phrenic nerve (Mitchell, Herbert, Baker & Basbaum, 1987), with different populations of cells being distinguished by whether they fired with either an inspiratory or expiratory rhythm.

We have recently developed a preparation that permits us to visualize directly, and record from, intact intramural paratracheal neurones present in the trachealis muscle of the rat. In the present study, we have investigated the firing characteristics and the currents responsible for the control of excitability in these cells. The possible implications of these findings to our understanding of the role of the intrinsic ganglia in the control of airway function are discussed.

METHODS

All experiments were performed on 14- to 18-day-old Sprague–Dawley rat pups from both sexes. Animals were stunned and then killed by cervical dislocation. The trachea between the base of the larynx and the bifurcation of the left and right bronchi was removed, cut mid-line along the length of its ventral surface and pinned out onto a small block of Sylgard (Dow Corning). The Sylgard block bearing the trachea was pre-bonded to a glass slide which formed the base of a Perspex recording chamber. The assembled chamber was then clamped to the stage of a Zeiss Ergoval microscope equipped with modulation contrast optics giving 320- and 640-fold magnification. The preparation was perfused at a rate of 6 ml/min with Krebs solution maintained at 33–34 °C using a remote thermostatically controlled heating coil. The Krebs solution was of the following composition (mM): NaCl, 112; KCl, 4·7; $MgCl_2$, 1·2; NaH_2PO_4, 1·2; $CaCl_2$, 2·5; $NaHCO_3$, 25; glucose, 11; gassed with 95% O_2–5% CO_2.

Impalements were made using electrodes with DC resistances between 90 and 130 MΩ, containing 2 M-potassium citrate solution (pH 7·3). In order to aid the placement of electrodes and

impalement of neurones, the final 3–6 mm of the electrodes were bent through an angle of 60 deg prior to filling. Discontinuous single-electrode voltage- and current-clamp recordings were made using an amplifier with a 30% current duty cycle (Axoclamp-2A) using a sampling frequency of 3–5 kHz.

When constructing current–voltage relationships, the values for the 'instantaneous' currents could not be measured directly, due to the presence of transient currents at the start of the voltage command. Estimation of the 'instantaneous' current flow was made by extrapolating the current measured after all transients had decayed back to time zero.

The limited frequency response obtainable when combining the discontinuous voltage-clamp technique with the use of high-resistance microelectrodes prevented adequate clamping of rapid currents such as those underlying the action potential. In order to overcome this problem when studying the current underlying the prolonged spike after-hyperpolarization, a 'hybrid' type of voltage-clamp technique was utilized. This entailed briefly switching the recording amplifier from voltage-clamp to 'bridge' mode. In 'bridge' mode, trains of action potentials were generated by passing brief intrasomal current pulses (5–15 ms) of sufficient intensity to elicit action potential discharge. At the end of the period of stimulation the amplifier was then switched back into voltage-clamp mode to permit measurement of the evoked slow post-spike currents. Action potential discharge was elicited using a brief series, rather than prolonged current pulses, as this minimized the activation of slow time-dependent currents. In addition, this was found to be a better method for inducing a consistent action potential discharge when the cells were superfused with solutions of different ionic composition.

Data were either stored on tape for future analysis (Racal Store 4DS) or displayed using a Tektronix storage oscilloscope (model D13) and a Gould pressure ink recorder (model 2200S). Numerical data are expressed as mean $\pm$ S.E.M.

Ionic substitution

In order to maintain Donnan equilibrium as well as osmolarity, solutions containing elevated potassium were made by substituting potassium sulphate and sodium gluconate for sodium chloride. Low-calcium-containing solutions were made by direct substitution with magnesium.

Drugs

4-Aminopyridine, barium chloride, cadmium chloride, caesium chloride and tetrodotoxin (TTX) were obtained from Sigma.

RESULTS

Recordings were made from more than 150 paratracheal neurones from Sprague–Dawley rat pups aged between 14 and 18 days. Resting membrane potentials recorded after an initial settling period were between -50 and -73 mV (mean $-57{\cdot}1 \pm 0{\cdot}73$ mV, $n = 68$).

Spontaneous synaptic activity

Approximately 50–60% of all neurones displayed spontaneous fast synaptic potentials (see Fig. 1*A*). In general, these potentials were small, ranging in amplitude from 3 to 10 mV, but occasionally large potentials leading to spike discharge were also observed. The amount of spontaneous synaptic activity varied considerably from one cell to another and, in general, appeared to be random in nature. However, a distinct pattern to the synaptic activity was occasionally seen, with a small burst of synaptic potentials being observed at regular intervals (see Fig. 1*B*). In all cases, hexamethonium (100 μM) or 0 Ca^{2+}, 3·2 mM-Mg^{2+} solutions, abolished all spontaneous synaptic activity. TTX (0·3–1 μM) reduced, though never totally abolished, the observed spontaneous synaptic activity, displaying a greater

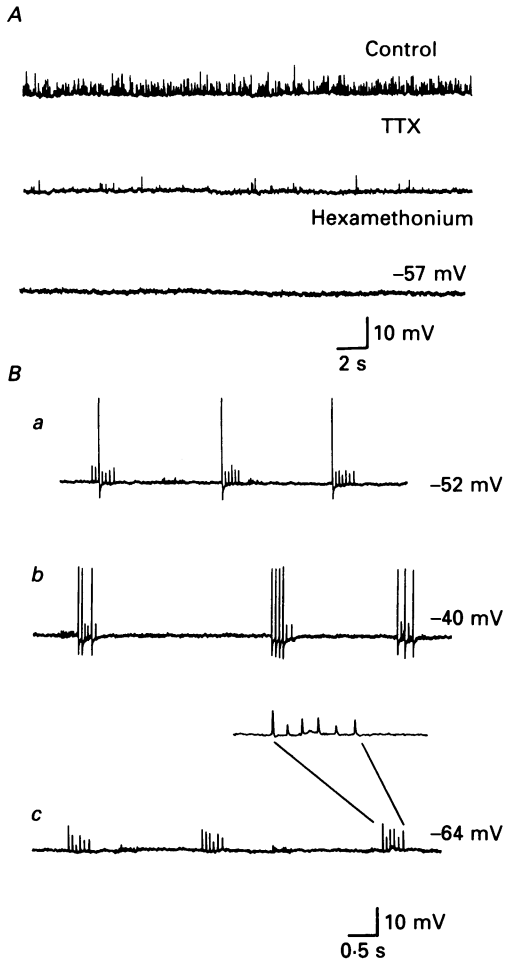

Fig. 1. Spontaneous synaptic potentials recorded from paratracheal neurones. *A*, random spontaneous fast EPSPs in a tonic-firing neurone. Synaptic activity was greatly reduced in the presence of TTX (330 nM, middle panel) and totally abolished in the presence of hexamethonium (100 μM, lower panel). Resting membrane potential -57 mV. *B*, another cell where the spontaneous synaptic activity consisted of small bursts of six fast synaptic potentials which repeated every 3–5 s. At resting membrane potential (-52 mV, *a*) the cell was only stimulated to fire in response to the largest of the synaptic potentials. When the cell was depolarized using intrasomal current injection, an increase in the frequency of spike discharge could be elicited (*b*). Hyperpolarization of the cell away from firing threshold led to inhibition of spike discharge and an increase in the amplitudes of the synaptic potentials (*c*). Note: action potentials were attenuated by the pen recorder.

potency in inhibiting the larger synaptic potentials. This indicates that at least some of the observed synaptic activity may be action-potential evoked.

Current firing characteristics

On the basis of the responses to intrasomal current injection, two patterns of neuronal firing were observed. These did not represent clearly distinct neuronal

subpopulations, rather they were the two extreme types of behaviour observed in the present study. At one extreme, and the most frequently observed characteristic (65–75% of cells), was burst-firing activity in response to prolonged intrasomal current injection. Typically, when stimulated at low current intensities (50–100 pA), these cells would only fire at the onset of current injection (see Fig. 2*A*). When the stimulating current was increased (100–300 pA), the cell would start to fire short, high-frequency bursts of action potentials for the period of stimulation (see Fig. 2*B*). Firing frequencies within these bursts were generally high (50–90 Hz) with an interburst interval of between 300 and 500 ms. Further increasing the stimulating current acted to prolong the duration of these bursts and also decreased the interburst interval (see Fig. 2*C*). At high current intensities (500–800 pA) the bursts would merge and the cell would fire tonically, at high frequencies, for the duration of current stimulation (see Fig. 2*D*). The long trains of action potentials generated in this way were invariably followed by a pronounced after-hyperpolarization, with an amplitude of between 10 and 20 mV, which persisted for up to 3 s (see Fig. 2*D*).

The other type of extreme firing characteristic seen in paratracheal neurones occurred in about 10–15% of the cells studied. These cells characteristically displayed longer after-hyperpolarization than the burst-firing cells (see later). In response to prolonged intrasomal current injection (50–100 pA), these cells again only fired at the start of current injection (see Fig. 2*E*). However, slightly raising the current intensity evoked tonic firing that was of a low frequency (1–5 Hz) and was not preceded by burst-firing behaviour (see Fig. 2*F*). Higher stimulating currents (500–1000 pA) increased firing rate to a maximum of between 10 and 15 Hz (see Fig. 2*G* and *H*). Following a period of prolonged firing in these cells, there was a prolonged after-hyperpolarization. However, this was usually considerably shorter than that observed following periods of firing in cells displaying bursting characteristics (see Fig. 2*H*).

Between these two extreme types of behaviour a number of cells responded with weak burst-firing behaviour, and had intermediate firing rates and after-hyperpolarization durations.

Sodium and calcium dependence of action potentials

The action potentials and after-hyperpolarizations of both burst- and tonic-firing paratracheal neurones exhibited a TTX-resistant component. In the presence of TTX (0·3–1 μM) the action potential amplitude was reduced, revealing a smaller, more slowly rising, TTX-resistant spike (see Fig. 3*A*). The after-hyperpolarization was largely unaffected by TTX (see Fig. 3*B*).

Superfusion with a mixture of TTX and 0 Ca^{2+}, high-Mg^{2+} solutions reversibly abolished both the remaining action potential and also the subsequent after-hyperpolarization (see Fig. 3*A* and *B*).

Current–voltage relationships

All of the paratracheal neurones studied displayed a characteristic sigmoidal current–voltage relationship. This resulted from the presence of an outward M-current activated by depolarization and of inward rectifier currents activated when the cell was hyperpolarized from resting potential.

M-current

Activation of this current resulted in marked outward rectification in the steady-state current–voltage relationship at membrane potentials less than −60 mV. This non-inactivating current displayed slow time- and voltage-dependent activation,

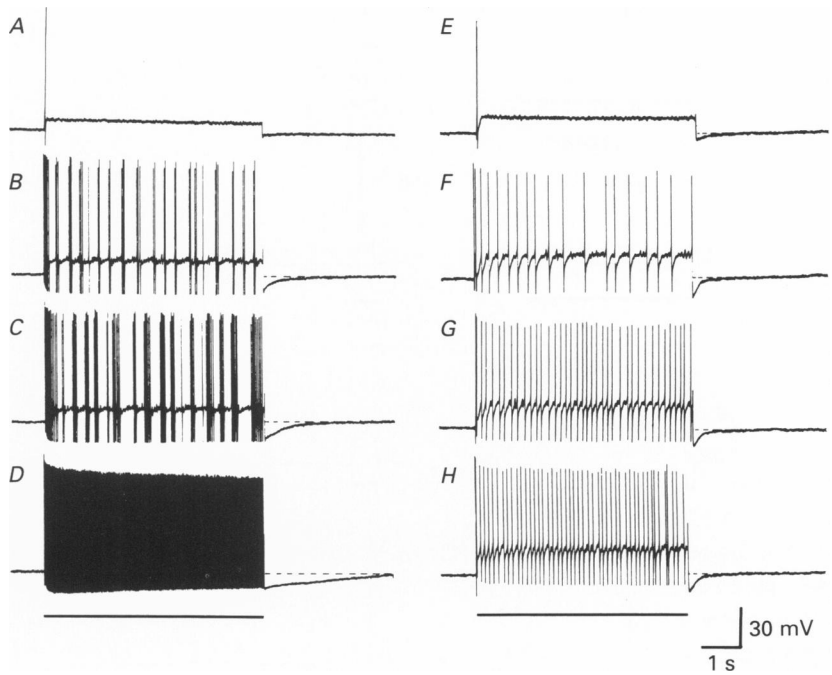

Fig. 2. The firing characteristics of paratracheal neurones stimulated by prolonged intrasomal current injection of increasing intensities. The traces in the left-hand column, *A–D*, were recorded from a burst-firing neurone. *A*, stimulation with low current intensities (150 pA, 5 s) only elicited firing at the onset of current injection. *B*, increasing the current intensity to 300 pA induced the cell to fire short high-frequency bursts of action potentials for the duration of current stimulation. *C*, further increasing the stimulating current to 500 pA increased the duration of these bursts and slightly decreased the interburst interval. *D*, at high current intensities (800 pA) the bursts of firing fused and the cell started to fire tonically at high frequencies for the duration of the stimulus. Trains of action potentials generated in this way were invariably followed by a prolonged after-hyperpolarization which persisted for up to 3 s and ranged in amplitude between 10 and 20 mV. Records *E–H* were obtained under similar conditions from a non-burst-firing cell. *E*, at low current intensities the cell again only fired at the start of the stimulus. Note the long spike after-hyperpolarization as compared to the cell in *A*. *F*, increasing the stimulus current induced low-frequency multiple firing. Further increases in stimulus intensity, records *G* and *H*, produced an increase in this discharge but never to the levels seen in the burst-firing neurones.

which resulted in a sag in the voltage response to depolarizing current injection and an overshoot and slow relaxation back to resting potential at the offset of current injection. To study this current, neurones were voltage clamped at a depolarized membrane potential of between −25 and −30 mV and subjected to a series of increasing amplitude hyperpolarizing steps (0·5–1 s, −10 mV increments). At the

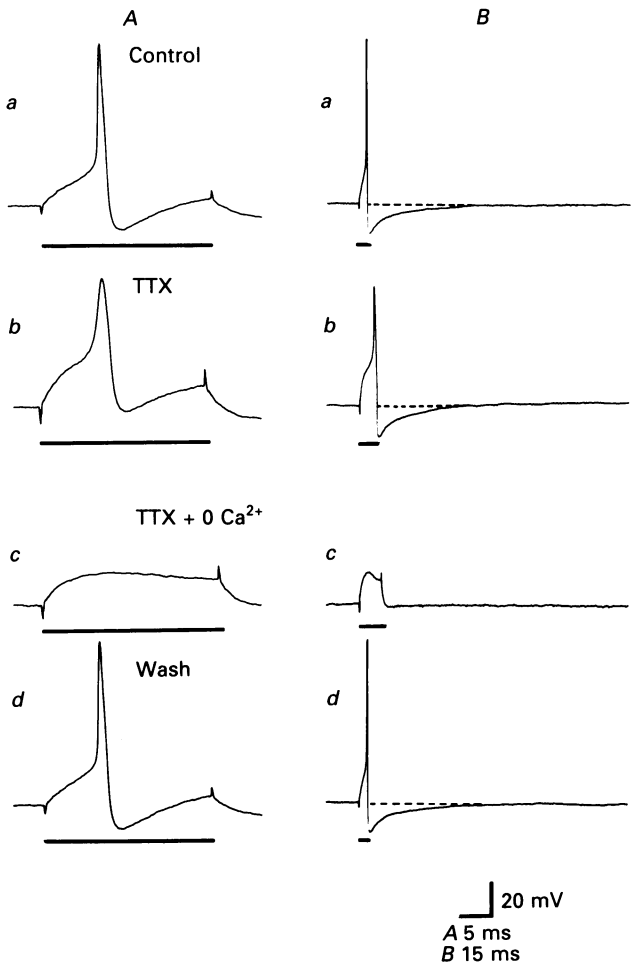

Fig. 3. Sodium and calcium dependence of the action potential (column *A*) and spike after-hyperpolarization (column *B*) in paratracheal neurones. *Aa* and *Ba*, control spike and after-hyperpolarization. In the presence of TTX (0·3–1 μM) the amplitude of the action potential was reduced but not abolished. By slightly raising the intensity of the stimulating current an improvement in the amplitude of the TTX-resistant spike could frequently be achieved (see *Ab*). Under these conditions the spike after-hyperpolarization was observed to be largely unaffected by TTX (see *Bb*). *Ac* and *Bc*, superfusion with Ca^{2+}-free and 0·3–1 μM-TTX-containing solutions abolished both the TTX-resistant action potential and the spike after-hyperpolarization. *Ad* and *Bd*, wash.

start of each voltage command, there was a near-instantaneous current step, which was then followed by a much slower inward current relaxation. Upon repolarization to −25 mV at the end of the voltage step, a similar sequence of 'instantaneous' and slow outward currents was observed.

The slow inward current relaxations initiated by hyperpolarizing steps were found to fit a single exponential and the rate of relaxation increased markedly at more

hyperpolarized potentials (see Fig. 4*C*). The mean time constant for the relaxations (from a holding potential of −30 mV) at −40, −50 and −60 mV calculated for four separate cells was 86·5 ± 4·3, 67·2 ± 3·8 and 49·7 ± 2·8 ms, respectively.

With hyperpolarizing steps of increasing amplitude, the size of the slow inward current relaxation first decreased, nulled, then at sufficiently hyperpolarized potentials reversed to become a slow outward current relaxation (see Fig. 4*B*). In cells with little slow inward rectification (or in cells where this current was inhibited by extracellular caesium ions; see later), the reversal potential for the M-current relaxation could be estimated from the point of intersection of the 'instantaneous' and steady-state current–voltage curves (see Fig. 4*B*). The mean null/reversal potentials for the current in control (4·7 mM) and elevated (20 mM) extracellular potassium-containing solutions were −85·1 ± 0·69 mV ($n = 9$) and −44·7 ± 1·16 mV ($n = 5$), respectively. This shift of approximately 40 mV in the equilibrium potential for the M-current agrees well with that predicted from the Nernst equation for a current carried exclusively by potassium ions.

Inhibition of the M-current

The effects of extracellular caesium and barium ions on the outward rectification and M-current relaxations were studied. Steady-state current–voltage curves were constructed under control conditions and in the presence of caesium and barium ions (using the same protocol as detailed in the previous section). Caesium chloride (1–3 mM) greatly reduced inward rectification (see later), while the outward rectification remained almost totally unaffected (see Fig. 5*A* and *B*). Subsequent addition of $BaCl_2$ (1 mM), either in the presence or absence of caesium, produced a large reduction in the steady outward current at −30 mV and reduced the amplitude, but not the time course, of the slow current relaxations associated with the M-current (see Figs 4*A* and 5*A*). Barium also reduced inward rectification (see later).

Inward rectifier current

Membrane hyperpolarization revealed marked inward rectification in all paratracheal neurones. In almost all cells, activation of this inward current occurred close to resting membrane potential between −55 and −70 mV. The exact potential at which inward rectification commenced was difficult to assess; as in most cases it overlapped with the activation range of the M-channels.

In order to examine the inward rectification under conditions where current flow through M-channels was minimal, cells were voltage-clamped at a potential of −60 mV. Cells were then subjected to a series of voltage steps of increasing amplitude (0·5–1 s, −10 mV increments). Stepping membrane potential in this way elicited an 'instantaneous' current flow, followed by a slow inward current relaxation ($\tau = 80$–160 ms). At the end of the voltage commands, repolarization to −60 mV elicited a similar 'instantaneous' current flow and a slow outward tail current as the inward rectifier current declined (see Figs 6*A* and 7*A*). The amplitude of the inward relaxation and the tail current increased as the command potential was made more negative (see Fig. 6*A*). The rate of current relaxation also increased with hyperpolarization: at −80 mV the mean time constant for the relaxation was

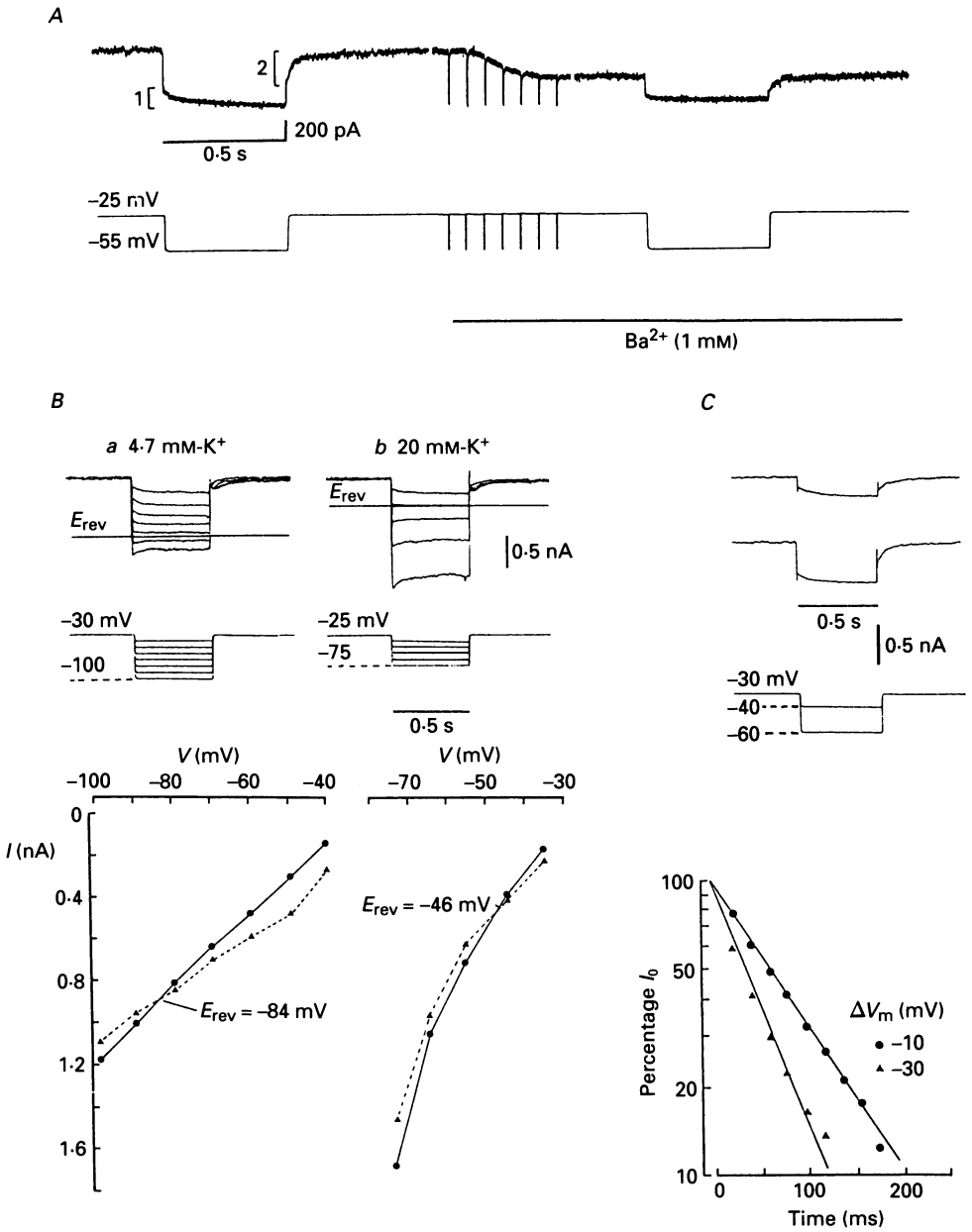

Fig. 4. The M-current in a burst-firing paratracheal neurone examined under voltage clamp. *A*, from a holding potential of −25 mV a voltage step to −55 mV was imposed for 500 ms. This produced a near-instantaneous flow of current through both 'leak' and M-channels open at −25 mV. This was followed by a slow inward current relaxation (1) as the M-channels closed in response to membrane hyperpolarization. At the end of the command step, a similar pattern of 'instantaneous' and slow current (2) relaxations was observed. Superfusion with $BaCl_2$ (1 mM) produced marked reduction in the M-current flowing at −25 mV and also reduced the amplitude of the slow inward and outward current relaxations. *B*, the ionic and voltage dependence of the M-current (holding

142·2 ± 4·7 ms ($n = 4$), while at −90 and −100 mV this value was reduced to 126·7 ± 5·4 ms ($n = 4$) and 87·2 ± 4·2 ms ($n = 4$), respectively.

In some cells, where the slow inward current relaxation and tail currents were small (it was never observed to be totally absent), inward rectification was still observed, but did not become pronounced until considerably more hyperpolarized potentials (> −80 mV).

Current–voltage curves were constructed by plotting the 'instantaneous' (see Methods) and steady-state currents evoked during voltage steps (see Fig. 6*B*). From such curves it was apparent that the observed inward rectification consisted of two components. The first displayed near-instantaneous activation, and resulted in inward rectification at potentials greater than −75 to −85 mV (see Fig. 6*B*). The second component showed much slower activation and produced rectification at all potentials from approximately −60 to −120 mV (see Fig. 6*B*).

The level of activation of the slow inward rectifier was examined by plotting 'instantaneous' minus steady-state current values as a function of membrane potential (see Fig. 6*C*). Activation of the slow inward rectifier current increased with membrane hyperpolarization from −60 mV, before reaching a peak at around −100 mV. With further hyperpolarization up to −120 mV, the amplitude of the inward current relaxation declined slightly, but was never observed to null or reverse (see Fig. 6*A* and *C*).

Inhibition by caesium and barium ions

Extracellular caesium (1 mM) inhibited both the 'instantaneous' and slow time- and voltage-dependent inward rectifier currents and produced a marked linearization of the 'instantaneous' and steady-state current–voltage relationships between −60 and −120 mV (see Fig. 7*B*).

Superfusion with barium (1 mM) also strongly inhibited the fast inward rectifier current (see Fig. 7*C*). However, at concentrations up to 1 mM, barium only slightly reduced the slow time-dependent inward rectifier current (see Fig. 7*C*). In the presence of caesium and barium the input resistance of all neurones was markedly

---

potential −30 mV). *a*, under control conditions (4·7 mM-K^+), increasing amplitude hyperpolarizing steps (500 ms, −10 mV increments) reduced, nulled and finally reversed the slow current relaxation associated with M-channel closure. *b*, in 20 mM-potassium the reversal potential for the slow inward current relaxation was shifted to more depolarized potentials. By plotting the 'instantaneous' (●) and the steady-state currents (▲) induced during the hyperpolarizing command steps for the cell shown in *a* and *b*, the equilibrium–reversal potential for the M-current could be determined. In 4·7 mM-potassium (left graph) the null potential was −84 mV, while in 20 mM-potassium (right graph) this value was shifted to −46 mV. *C*, kinetics of the M-current relaxations. Upper traces, M-current relaxations in response to voltage steps to −40 and −60 mV respectively (holding potential −30 mV). Graph (below) shows current relaxation plotted against time. Lines are least-squares fits to data for cell shown. The zero-time intercept (I_0) was calculated as the difference between the 'instantaneous' and steady-state values. The different values of I_0 were used to normalize data in each case, relaxation currents being plotted as $\log_{10}$% of I_0 *vs.* time. M-current relaxations were best fitted by a single exponential ($r = 0{\cdot}998$ at −40 mV and 0·990 at −60 mV), with relaxation time constants of 86 ms at −40 mV and 51 ms at −60 mV.

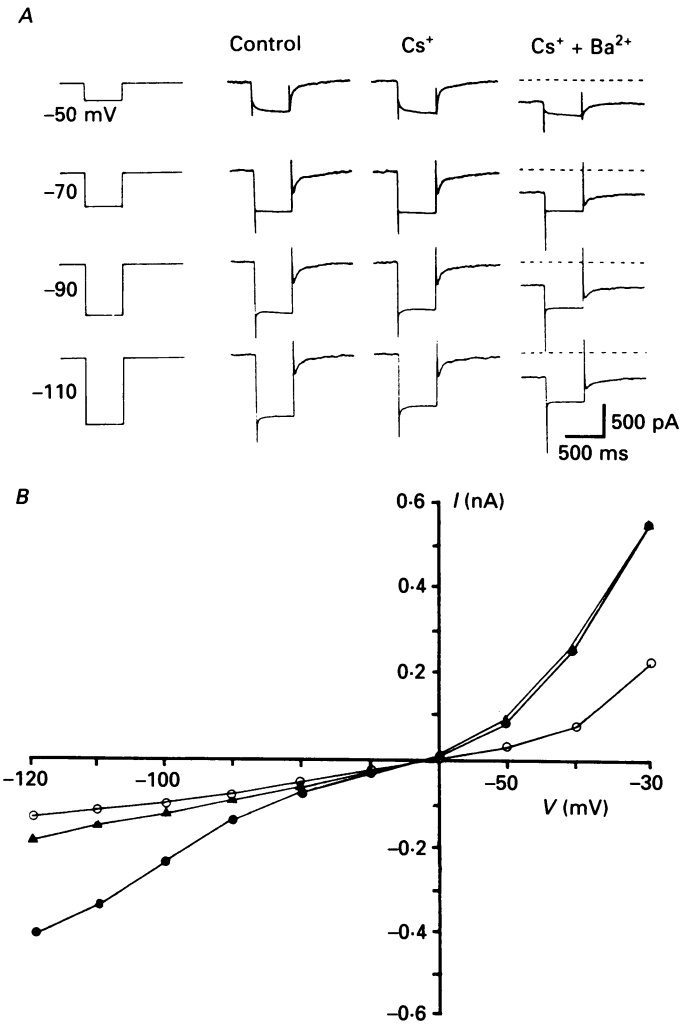

Fig. 5. The inhibitory actions of Cs^+ and Ba^{2+} ions on the M-current in a paratracheal neurone. *A*, from a holding potential of −30 mV the cell was subjected to a series of 500 ms duration negative command pulses of increasing amplitude. With increasing hyperpolarization, the slow inward current relaxation associated with M-channel closure decreased, then reversed to become a slow outward relaxation. The null/reversal point for M-current was approximately −85 mV. Superfusion with CsCl (2 mM) inhibited the inward rectifier current but had no effect upon the M-current. Superfusion with CsCl (2 mM) and $BaCl_2$ (1 mM) produced an inhibition of the M-current and a further decrease in inward rectification. *B*, the current–voltage (*I–V*) relationships for the cell shown in *A*. Under control conditions (●) the cell displayed a characteristic sigmoidal *I–V* curve due to the presence of both outward and inward rectifying currents. In the presence of CsCl (▲, 2 mM) inward rectification in the *I–V* relationship at hyperpolarized potentials (> −60 mV) was reduced, but there was no observable reduction in the M-current. In the presence of both CsCl (2 mM) and $BaCl_2$ (1 mM) (○) the M-current was inhibited and there was also a further reduction in inward rectification. This resulted in an increase in the input resistance of the cell and an almost linear *I–V* relationship between −45 and −120 mV.

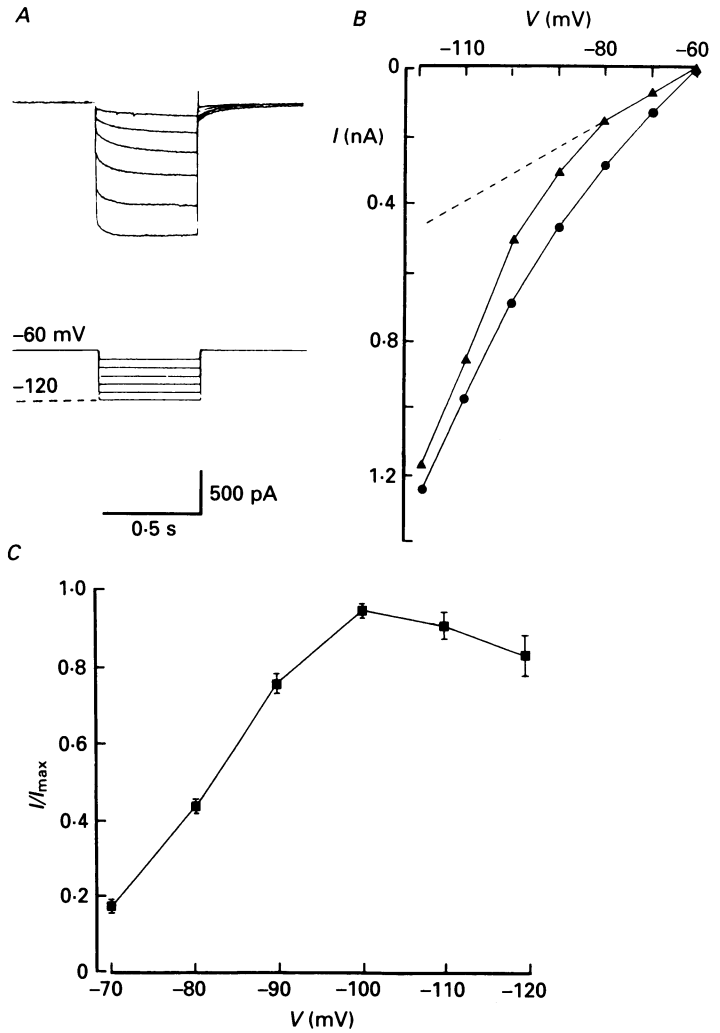

Fig. 6. Inward rectification in a typical paratracheal neurone. *A*, from a holding potential of −60 mV, negative voltage steps (10 mV increments) revealed inward rectification and a slow inward current relaxation in membrane current. At the end of the voltage steps the initial 'instantaneous' current flow was followed by a slow outward current relaxation as the inward rectifier current inactivated. *B*, the 'instantaneous' (▲) and steady-state (●) current–voltage relationships for the cell shown in *A*. From these curves it is evident that the observed inward rectification consists of two components. Examination of the instantaneous current–voltage relationship reveals the presence of an inwardly rectifying current activated at potentials greater than −80 mV. The steady-state current–voltage relationship on the other hand shows voltage-dependent inward rectification from all potentials negative to the holding potential (−60 mV). At potentials less than −80 mV the rectification results almost exclusively from activation of the slow time-dependent inward rectifier current which manifests itself as an inward relaxation in the current records shown in *A*. *C*, activation of the slow inward rectifier current. Current flow resulting from activation of the slow inward rectifier (steady-state minus 'instantaneous' currents), represented as a fraction of the peak current, is plotted as a function of membrane potential. Values in each case are means ± S.E.M. for between eleven and fifteen observations. From the curve it can be seen that peak activation of the slow inward rectifier current occurs around −100 mV then declines slightly with further hyperpolarization.

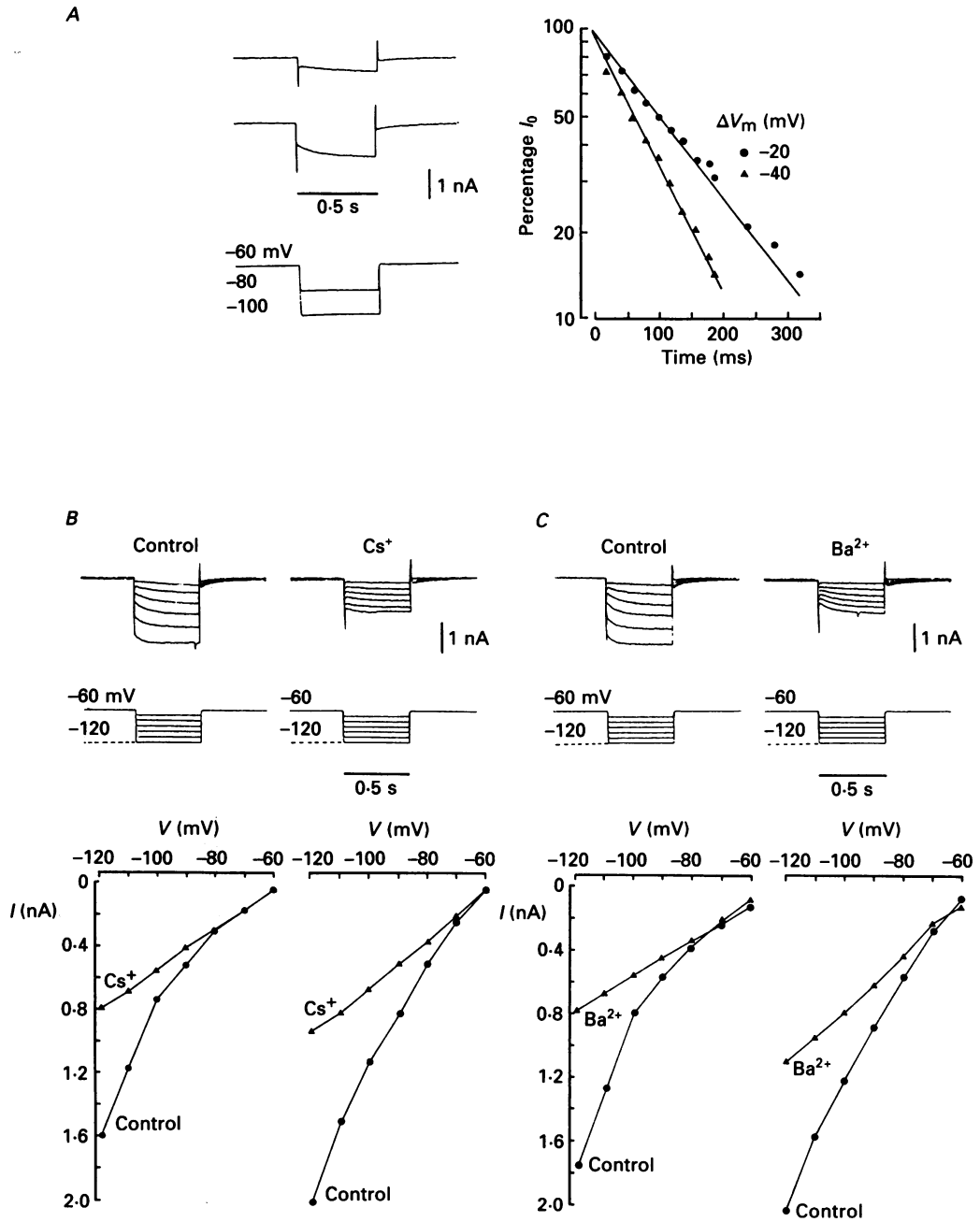

Fig. 7. *A*, kinetics of the current relaxations underlying the slow time-dependent inward rectifier current. Traces (upper left) show inward current relaxations initiated by hyperpolarization to −80 and −100 mV. Graph (upper right) is a semilogarithmic plot of current relaxations against time. Lines are least-squares fits to data from traces on left of graph. The zero-time intercept (I_0) was calculated as the difference between the 'instantaneous' and steady-state current values. The different values of I_0 were used to normalize data in each case, relaxation currents being plotted as $\log_{10}$% of I_0 *vs.* time.

increased and the current–voltage relationship was largely linear between −45 and −120 mV (see Fig. 5*B*).

The spike after-hyperpolarization

The after-hyperpolarization following a single action potential in paratracheal neurones typically persisted for between 90 and 500 ms and ranged in amplitude between 5 and 15 mV. In general, the after-hyperpolarization in tonic-firing neurones was longer than that seen in the burst-firing cells. Mean duration for burst-firing cells was 114 ± 4·7 ms ($n = 42$) while that for tonic-firing cells was 315 ± 17·5 ms ($n = 19$). In all cells, the amplitude and duration of the after-hyperpolarization increased markedly as the number and frequency of the preceding action potentials increased. The current underlying the after-hyperpolarization (I_{AHP}) was studied using a 'hybrid' voltage-clamp technique (see Methods) and was found to be linearly related to the membrane potential at which it was elicited. With membrane hyperpolarization from rest, the outward current decreased and nulled at between −83 and −91 mV (mean −86·5 ± 0·8 mV, $n = 14$). Further hyperpolarization reversed the current leading to inward current flow (Fig. 8*A*).

The ionic dependence of I_{AHP} was also examined in solutions containing 12·5 and 20 mM-potassium (see Fig. 8*A* and *B*). The mean null/reversal potentials recorded in these solutions were −59·3 ± 1·11 mV ($n = 3$) and −46·4 ± 1·15 mV ($n = 3$), respectively. These values agree well with those predicted by the Nernst equation for a current carried exclusively by potassium ions, with the reversal potential shifted by 63·6 mV for a 10-fold increase in extracellular potassium concentration.

Removal of extracellular calcium abolished the after-hyperpolarization following both single or trains of action potentials. Superfusion with low-calcium-containing solutions (0·25 mM) markedly reduced the size and duration of the outward current underlying the after-hyperpolarization (see Fig. 9). The mean reduction in the duration of the outward current flow was 62 ± 5·15% ($n = 4$) and the reduction in peak current was 52·7 ± 4·64% ($n = 4$). Raising extracellular calcium produced an increase in I_{AHP}. In the presence of Ca^{2+} (5 mM) the mean increase in duration of I_{AHP} was 135 ± 6·1% ($n = 4$), while the increase in peak current flow was 105·6 ± 0·92% ($n = 5$).

Current relaxations were best fitted by a single exponential ($r = 0{\cdot}978$ at −80 mV and 0·994 at −100 mV), with relaxation time constants of 146 ms at −80 mV and 94·5 ms at −100 mV. *B* and *C*, the inhibitory actions of extracellular caesium and barium ions, respectively, on the 'instantaneous' and slow time-dependent inward rectifier currents. All membrane currents were recorded in response to negative voltage steps from a holding potential of −60 mV. Caesium (1 mM, *B*) and barium (1 mM, *C*) both strongly inhibited the 'instantaneous' inward rectifier current, resulting in a reduction in inward rectification and linearization of the 'instantaneous' current–voltage relationship (see traces and left-hand graphs in *B* and *C*). The slow time-dependent inward rectifier was also strongly inhibited by caesium (1 mM), which largely abolished the inward rectification seen in the steady-state current–voltage relationship under control conditions (see right-hand graph in *B*). In the presence of barium (1 mM) the time-dependent component of inward rectification was reduced, but not to the same degree as seen in the presence of caesium (see traces and right-hand graph in *C*).

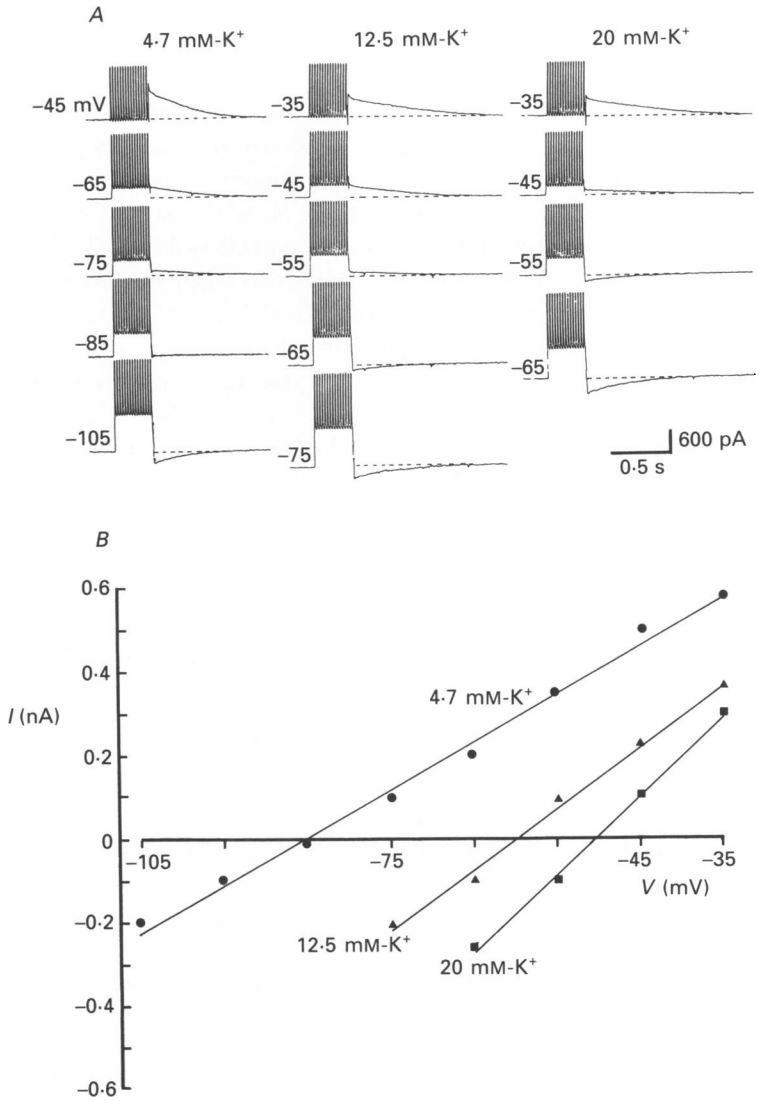

Fig. 8. The ionic and voltage dependence of the current underlying the prolonged spike after-hyperpolarization (I_{AHP}) in a tonic-firing paratracheal neurone. *A*, recordings were made using a 'hybrid' voltage-clamp technique (see Methods). From a given holding potential the recording amplifier was switched from voltage clamp into standard 'bridge' recording mode and a train of action potentials evoked by passing a series of intrasomal current pulses (10 ms, 40 Hz) of sufficient intensity to elicit firing. At the end of the train of spikes the amplifier was then switched back to voltage-clamp mode to permit recording of the evoked current. Under control conditions (4·7 mM-K^+) the amplitude of I_{AHP} was found to be linearly related to membrane potential and had a reversal potential of −85·5 mV (see *B*). In elevated-potassium-containing solutions (12·5 and 20 mM) I_{AHP} was slightly prolonged and the reversal potential was shifted to more depolarized levels. *B*, the voltage dependence of I_{AHP} for the cell shown in *A* was plotted for each different potassium-containing solution. In order to reduce the error in measuring, the current measurements were made 100 ms after the train of action potentials. In all cases the

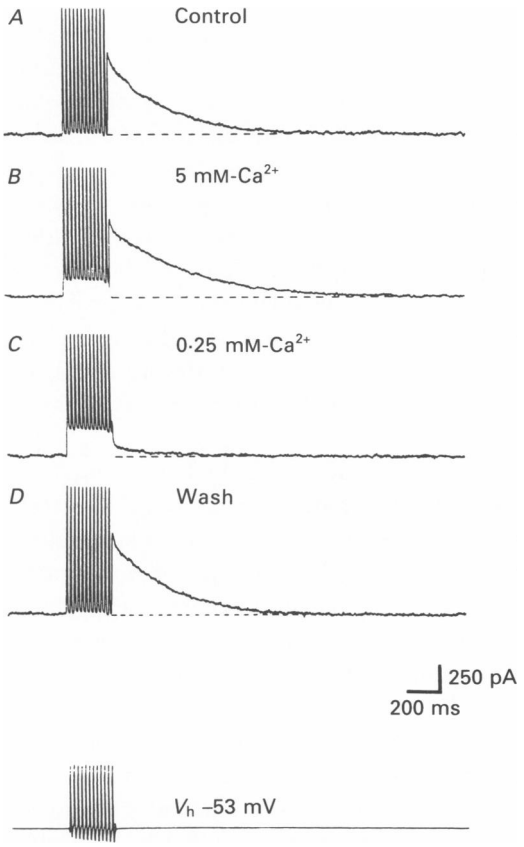

Fig. 9. Calcium dependence of the current underlying the prolonged spike after-hyperpolarization (I_{AHP}) in a tonic-firing paratracheal neurone. *A*, recordings were made using a 'hybrid' voltage-clamp technique (see Methods). From voltage-clamp recording at a holding potential of −53 mV the recording amplifier was briefly switched to standard 'bridge' mode and a train of action potentials generated by passing brief (10 ms, 40 Hz) intrasomal current pulses. At the end of the train the amplifier was returned to voltage-clamp mode. *B*, in the presence of elevated-calcium (5 mM)-containing solutions the duration of the current underlying the after-hyperpolarization was prolonged, whereas the amplitude of the current was almost unaffected. *C*, in low-calcium (0·25 mM), elevated-magnesium (3·45 mM)-containing solutions, both the amplitude and the duration of the I_{AHP} were greatly reduced. *D*, wash-out to control conditions.

DISCUSSION

The findings of the present study demonstrate that the parasympathetic intramural ganglia of the rat trachea contain neurones which display a high degree

amplitude of I_{AHP} was linearly related to the membrane potential at which it was elicited. In 4·7, 12·5 and 20 mM-K^+-containing solution, least-squares fits of the raw data produced the regression coefficients of 0·996, 0·997 and 0·998 and reversal potentials of −85·5, −59·5 and −50·5 mV, respectively. The values for the reversal potentials show reasonable agreement with the values predicted by the Nernst equation for a current carried exclusively by potassium ions.

of electrophysiological specialization, and as such, may act as sites of integration and/or modulation of the input from extrinsic nerves. Furthermore, where the plexus of intrinsic ganglia remained largely intact, spontaneous synaptic activity was frequently observed. Spontaneous activity consisted largely of subthreshold, and occasionally suprathreshold, fast cholinergic potentials. It is likely that the majority of the small synaptic potentials arose as a result of spontaneous transmitter release from extrinsic nerve terminals. However, the presence of rhythmic bursts of TTX-sensitive synaptic potentials in a number of cells, under conditions where the extrinsic nerves had been separated from their cell bodies, suggests that at least a proportion of the synaptic activity was the result of intrinsic synaptic interactions between paratracheal neurones within these ganglia. Such synapses would permit a degree of local, as well as extrinsic, control of airway function; this type of activity has also been demonstrated in the enteric nervous system of the gut (see Costa & Furness, 1982).

The presence of high levels of subthreshold fast synaptic activity has also been observed in an *in vivo* study of cat paratracheal ganglia (Mitchell *et al.* 1987). In this report on cat ganglia, two cell types were distinguished which fired in a phasic/bursting manner, similar to the majority of rat paratracheal neurones in the present investigation. The bursts of firing in the two types of cat ganglion cells were synchronized with either inspiration or expiration. Generation of this discharge was attributed to synchronization of the multiple subthreshold synaptic inputs from preganglionic nerves. In the present study, we were not in a position to determine whether rat paratracheal neurones fired with a similar respiratory rhythm. However, from our study of the basic properties of these neurones, it would appear that the burst/phasic behaviour may be an inherent feature of these cells, which results from the complex underlying intrinsic membrane currents. Therefore, the intrinsic nerves may generate their own burst firing pattern which is activated or synchronized to inspiration or to expiration by either extrinsic nerves or through local reflex mechanisms.

In order to understand better the potential of these neurones to autoregulate their excitability, we examined the mechanisms underlying the different membrane currents present in these cells. All of the paratracheal neurones studied exhibited an M-current that resulted in outward rectification in the current–voltage relationship at depolarized potentials. This was similar to the M-current first identified in large (B) cells of frog lumbar sympathetic ganglia (Brown & Adams, 1980) and subsequently in other sympathetic and central neurones (for review see Brown, 1988). The M-current exerts a clamping action upon membrane potential by acting to oppose prolonged membrane depolarization. This, together with the presence in the majority of paratracheal neurones of an additional slow inward rectifier current which opposes membrane hyperpolarization, raises the possibility that these two currents may act in concert and be responsible for setting the resting membrane potential of these cells. In the present study, the activation points for the two currents were very similar and in some cells appeared to overlap slightly. Therefore, the membrane potential may be effectively squeezed into the narrow potential range where the effects of these two currents are minimal or cancel each other out. Indeed, the resting membrane potentials observed in the majority of rat paratracheal

neurones were found to lie within this range (−55 to −65 mV). Small changes in the level of activation of either of these currents would, therefore, produce a sensitive mechanism for adjusting resting membrane potential and hence, the medium or long-term excitability of these cells with minimal expenditure of metabolic energy, since one current would be activating as the other was de-activating.

Both the 'instantaneous' and slow inward rectifier currents in paratracheal neurones, like all other inward rectifiers studied so far, were strongly inhibited by low concentrations of caesium ions. The 'instantaneous' component of inward rectification in paratracheal neurones, unlike the slow component, was strongly inhibited by both caesium and barium ions. It seems unlikely that this rectification resulted from current flow through slow inward rectifier channels open at rest, as the current only displayed significant activation at potentials greater than −80 mV. The behaviour of the 'instantaneous' component of rectification and its sensitivity to barium ions was similar to that of the classical anomalous rectifier currents in marine eggs and skeletal muscle (Hagiwara, Miyazaki, Moody & Patlak, 1978; Standen & Stanfield, 1978).

The slow inward rectifier current was distinct from the 'instantaneous' rectifier and the anomalous rectifiers in striated muscle, marine eggs and cortical neurones (Hagiwara, Miyazaki & Rosenthal, 1976; Gay & Stanfield, 1977; Constanti & Galvan, 1983) in that it was largely insensitive to barium ions. This insensitivity to barium, and also the finding that the current did not reverse near the potassium equilibrium potential, indicates that the slow inward rectifier in paratracheal neurones may be similar to I_Q, I_H and I_H–I_f–I_{k2} (Brown & DiFrancesco, 1980; DiFrancesco & Ojeda, 1980; Halliwell & Adams, 1982; Mayer & Westbrook, 1983; Crepel & Penit-Soria, 1986).

Another current which may act to regulate excitability in rat paratracheal neurones is the post-spike calcium-activated potassium current ($I_{K,Ca}$). This outward current, like that described in many other neurones (for example see Nishi & North, 1973; Fowler, Greene & Weinreich, 1985; Allen & Burnstock, 1987), was activated by calcium entry during the action potential and was responsible for the prolonged after-hyperpolarization. Similar prolonged after-hyperpolarizations have been described in neurones from ferret, rabbit and cat paratracheal ganglia (Cameron & Coburn, 1984; Fowler & Weinreich, 1986; Mitchell *et al.* 1987), but have only been demonstrated to be calcium dependent in the ferret (Cameron & Coburn, 1982). The size and duration of the prolonged after-hyperpolarization was found to be significantly smaller in burst-firing than in tonic-firing rat paratracheal neurones. However, even in the tonic-firing cells, the magnitude of the prolonged after-hyperpolarization was considerably shorter than that observed in some of the highly refractory AH-type cells found in, for example, mammalian enteric and intracardiac ganglia (Morita, North & Tokimasa, 1982; Allen & Burnstock, 1987). In rat paratracheal neurones, particularly burst-firing cells, the after-hyperpolarization increased dramatically following a train of action potentials and may act to control the duration of each burst of firing. In addition, we also observed a transient outward current similar to the A-current (T. G. J. Allen & G. Burnstock, unpublished observation) which was most pronounced in tonic-firing cells that may also act to control rates of firing in these cells.

In conclusion, the present study of the electrophysiological properties of rat paratracheal neurones shows that these cells have considerable intrinsic electrophysiological complexity. This may allow subtle modulation of the effects of extrinsic nervous input by paratracheal neurones, or may even permit some local control of aspects of airway function by local reflex mechanisms. We hope to use the current preparation to study the synaptic interactions occurring within these ganglia and to examine how the intrinsic properties of the intramural neurones may be influenced by different patterns of synaptic stimulation.

This work was supported by grants from the Asthma Research Council and the Medical Research Council. The authors would also like to thank Dr F. A. Cribbin for editorial assistance in the preparation of this manuscript.

REFERENCES

ALLEN, T. G. J. & BURNSTOCK, G. (1987). Intracellular studies of the electrophysiological properties of cultured intracardiac neurones of the guinea-pig. *Journal of Physiology* **388**, 349–366.

BAKER, D. G. (1986). Parasympathetic motor pathways to the trachea: recent morphologic and electrophysiologic studies. *Clinical Chest Medicine* **7**, 223–229.

BAKER, D. G., MCDONALD, D. M., BASBAUM, C. B. & MITCHELL, R. A. (1986). The architecture of nerves and ganglia of the ferret trachea as revealed by acetylcholinesterase histochemistry. *Journal of Comparative Neurology* **246**, 513–526.

BALUK, P., FUJIWARA, T. & MATSUDA, S. (1985). The fine structure of the ganglia of the guinea-pig trachea. *Cell and Tissue Research* **239**, 51–60.

BALUK, P. & GABELLA, G. (1989). Ganglion neurones in the rat trachea lack sympathetic input and some of them partially express a noradrenergic phenotype. *Journal of Physiology* **416**, 16*P*.

BROWN, D. A. (1988). M currents. In *Ion Channels*, vol. 1, ed. NARAHASHI, T. pp. 55–94. Plenum Press, New York.

BROWN, D. A. & ADAMS, P. R. (1980). Muscarinic suppression of a novel voltage-sensitive K^+-current in a vertebrate neurone. *Nature* **283**, 673–676.

BROWN, D. A. & DIFRANCESCO, D. (1980). Voltage-clamp investigators of membrane currents underlying pace-maker activity in rabbit sino-atrial node. *Journal of Physiology* **308**, 331–351.

CAMERON, A. R. & COBURN, R. F. (1982). Calcium dependence of the afterhyperpolarization of type A cells of the ferret paratracheal ganglion. *Federation Proceedings* **41**, 1356.

CAMERON, A. R. & COBURN, R. F. (1984). Electrical and anatomical characteristics of the cells of the ferret paratracheal ganglion. *American Journal of Physiology* **246**, C450–458.

CHIANG, C.-H. & GABELLA, G. (1986). Quantitative study of the ganglion neurons of the mouse trachea. *Cell and Tissue Research* **246**, 243–252.

COBURN, R. F. & KALIA, M. P. (1986). Morphologic features of spiking and non-spiking cells in the paratracheal ganglion of the ferret. *Journal of Comparative Neurology* **254**, 341–351.

COBURN, R. F. & TOMITA, T. (1973). Evidence for noradrenergic inhibitory nerves in the guinea-pig trachealis muscle. *American Journal of Physiology* **224**, 1072–1080.

COLEMAN, R. A. & LEVY, G. P. (1974). A non-adrenergic inhibitory nervous pathway in guinea-pig trachea. *British Journal of Pharmacology* **52**, 167–174.

CONSTANTI, A. & GALVAN, M. (1983). Fast inward-rectifying current accounts for anomalous rectification in olfactory cortex neurones. *Journal of Physiology* **385**, 153–178.

COSTA, M. & FURNESS, J. B. (1982). Nervous control of intestinal motility. In *Handbook of Experimental Pharmacology*, vol. 59, *Mediators and Drugs in Gastrointestinal Motility. I. Morphological Basis and Neurophysiological Control*, ed. BERTACCINI, G., pp. 279–382. Springer, Berlin.

CREPEL, F. & PENIT-SORIA, J. (1986). Inward rectification and low threshold calcium conductance in rat cerebellar Purkinje cells. An *in vitro* study. *Journal of Physiology* **372**, 1–23.

DEY, R. D., SHANNON, W. A. JR & SAID, S. I. (1981). Localization of VIP-immunoreactive nerves in airways and pulmonary vessels of dogs, cats and human subjects. *Cell and Tissue Research* **220**, 231–238.

DIAMOND, L. & O'DONNELL, M. (1980). A non-adrenergic inhibitory pathway to the feline airways. *Science* **208**, 185–188.

DIFRANCESCO, D. & OJEDA, C. (1980). Properties of the current i_f in the sino-atrial node of the rabbit compared with those of i_{k2} in Purkinje fibres. *Journal of Physiology* **308**, 353–367.

ELFMAN, A. G. (1943). The afferent parasympathetic innervation of the lungs and trachea of the dog. *American Journal of Anatomy* **72**, 1–28.

FISHER, A. W. F. (1964). The intrinsic innervation of the trachea. *Journal of Anatomy* **98**, 117–124.

FOWLER, J. C., GREENE, R. & WEINREICH, D. (1985). Two calcium-sensitive spike after-hyperpolarizations in visceral sensory neurones of the rabbit. *Journal of Physiology* **365**, 59–75.

FOWLER, J. C. & WEINREICH, D. (1986). Electrophysiological membrane properties of paratracheal ganglion neurons of the rabbit. *Society for Neuroscience Abstracts* **11**, 1182.

GAY, L. A. & STANFIELD, P. R. (1977). Cs^+ causes a voltage-dependent block of inward K^+ currents in resting skeletal muscle fibres. *Nature* **267**, 169–170.

HAGIWARA, S., MIYAZAKI, S., MOODY, W. & PATLAK, J. (1978). Blocking effects of barium and hydrogen ions on the potassium current during anomalous rectification in the starfish egg. *Journal of Physiology* **279**, 167–185.

HAGIWARA, S., MIYAZAKI, S. & ROSENTHAL, N. P. (1976). Potassium current and the effect of cesium on this current during anomalous rectification of the egg cell membranes of a starfish. *Journal of General Physiology* **67**, 621–638.

HALLIWELL, J. V. & ADAMS, P. R. (1982). Voltage-clamp analysis of muscarinic excitation in hippocampal neurones. *Brain Research* **250**, 71–92.

HONJIN, R. (1954). On the ganglia and nerves of the lower respiratory tract of the mouse. *Journal of Morphology* **95**, 263–288.

HONJIN, R. (1956). On the nerve supply of the lungs of the mouse with special references to the structure of the peripheral vegetative nervous system. *Journal of Comparative Neurology* **105**, 587–625.

LANDOIS, L. (1885). *A Textbook of Human Physiology*. Translated by W. Stirling, vol. 1, 4th edn, pp. 217–225. Charles Griffin, London.

LARSELL, O. (1922). The ganglia, plexuses and nerve-terminations of the mammalian lung and pleura pulmonalis. *Journal of Comparative Neurology* **35**, 97–130.

LUNDBERG, J. M. & SARIA, A. (1987). Polypeptide-containing neurons in airway smooth muscle. *Annual Review of Physiology* **49**, 557–572.

MAYER, M. L. & WESTBROOK, G. L. (1983). A voltage-clamp analysis of inward (anomalous) rectification in mouse spinal sensory ganglion neurones. *Journal of Physiology* **340**, 19–45.

MITCHELL, R. A., HERBERT, D. A., BAKER, D. G. & BASBAUM, C. B. (1987). In vivo activity of tracheal parasympathetic ganglion cells innervating tracheal smooth muscle. *Brain Research* **437**, 157–160.

MORITA, K., NORTH, R. A. & TOKIMASA, T. (1982). The calcium-activated potassium conductance in guinea-pig myenteric neurones. *Journal of Physiology* **329**, 341–354.

NISHI, S. & NORTH, R. A. (1973). Intracellular recordings from the myenteric plexus of the guinea-pig ileum. *Journal of Physiology* **231**, 471–491.

PACK, R. J., AL-UGAILY, L. H. & WIDDICOMBE, J. G. (1984). The innervation of the trachea and extrapulmonary bronchi of the mouse. *Cell and Tissue Research* **238**, 61–68.

RICHARDSON, J. B. & BELAND, J. (1976). Nonadrenergic inhibitory nervous system in human airways. *Journal of Applied Physiology* **41**, 764–771.

RICHARDSON, J. B. & BOUCHARD, T. (1975). Demonstration of a nonadrenergic inhibitory nervous system in the trachea of the guinea-pig. *Journal of Allergy and Clinical Immunology* **56**, 437–480.

SMITH, R. B. & TAYLOR, I. M. (1971). Observations on the intrinsic innervation of the guinea-pig tracheobronchial smooth muscle. *Neuroscience Letters* **34**, 247–251.

STANDEN, N. B. & STANFIELD, P. R. (1978). A potential- and time-dependent blockade of inward rectification in frog skeletal muscle fibres by barium and strontium ions. *Journal of Physiology* **280**, 169–191.

UDDMAN, R., ALUMETS, J., DENSERT, O., HÅKANSON, R. & SUNDLER, F. (1978). Occurrence and distribution of VIP nerves in the nasal mucosa and tracheobronchial wall. *Acta otolaryngologica* **86**, 443–448.

YIP, P., PALOMBINI, B. & COBURN, R. F. (1981). Inhibitory innervation to the guinea-pig trachealis muscle. *Journal of Applied Physiology* **50**, 374–383.